Microchimica Acta (2019) 186:628
https://doi.org/10.1007/s00604-019-3719-8

ORIGINAL PAPER

Ultrasensitive electroluminescence biosensor for a breast cancer marker microRNA based on target cyclic regeneration and multi-labeled magnetized nanoparticles

Dongli Chen[1] · Meng Zhang[1] · Fenyue Zhou[1] · Hong Hai[1,2] · Jianping Li[1,2]

Received: 3 March 2019 / Accepted: 31 July 2019

Abstract

An electrochemiluminescent (ECL) biosensor is described for the determination of the breast cancer biomarker microRNA. The method is based on the amplification via target cyclic regeneration through a system of hairpin DNA probes, primers, and Klenow fragment of DNA polymerases combined with CdTe quantum dots (QDs) and gold nanoparticles. The assay is performed by exploiting the luminescence properties of CdTe-QDs and $K_2S_2O_8$ as a co-reactive agent to increase the ECL signal. It was successfully applied to ECL-based detection of a 20-mer microRNA. The sensor has a linear response in the 0.1 fM to 0.2 pM microRNA concentration range and a detection limit as low as 33 aM. The assay has been applied to the determination of microRNA spiked in serum samples, and recoveries ranged from 94.4 to 100.5%.

Keywords Biosensor · Electrochemiluminescence · Breast cancer · MicroRNA · Quantum dots · Polymerase · Enzyme-assistant · Signal amplification · Cyclic regeneration · Serum samples

Introduction

MicroRNA is a specific biomarker for breast cancer, and the use of the diacrisis of cancer has been widely researched because of the close association of expression levels with cancer burden and malignant progression [1–4]. High levels of related microRNA expression are usually discovered in most breast-cancer cases but are rarely detected when the patient is healthy [5]. As a result, the exploration of microRNA is very important for understanding and identifying the correct therapeutic and diagnostic decisions to breast-cancer cases [6, 7].

Thus, various modern techniques for microRNA detection, such as Northern blots [8, 9] and microarrays [10], are widely employed; however, large sample sizes and improved sensitivity and specificity are required for the application of these methods, hindering practical use of these methods within clinical settings. Although microRNA is frequently detected by real-time PCR [11, 12], an outstanding challenge is the accuracy of the results, which is significantly influenced by sample preparation, reagent quality, primer design, and experimental procedure. Fluorescent reporter [13] techniques have been successfully applied to detect and image intracellular microRNA; however, the application of these approaches is also significantly limited by the light scattering in the sample, excitation source fluctuations, and requirement of correct fluorescence intensity needed for such fluorescence-linked assays [14]. In comparison with various microRNA detection techniques, electrochemiluminescence (ECL) represents one of the most diverse bioassay methods because of its manageability and simplistic optical setup [15]. Unfortunately, using ECL alone is not sufficient to accurately detect and diagnose cancer early due to insufficient detection sensitivity. Various signal amplification strategies have been studied to overcome this limitation and further improve the accuracy of early cancer detection. Enzyme-assisted amplification is widely used for the development of ultrasensitive detection. Hybridization chain reactions [16, 17], rolling circle amplifications (RCA) [18], and the use of endonucleases [19] or exonucleases [20,

✉ Hong Hai
583776610@qq.com

✉ Jianping Li
likianping@263.net

[1] College of Chemistry and Bioengineering, Guilin University of Technology, Guangxi 541004, China

[2] Guangxi Key Laboratory of Electrochemical and Magnetochemical Function Materials, Guangxi 541004, China

Published online: 15 August 2019

21] have also been employed to improve the performance of sensors. Unfortunately, RCA is often limited by its dependence on inefficient enzymes and time-consuming and costly steps to prepare the required circular oligomer templates. Using endonucleases and exonucleases is also limited to specific temperature ranges and the need for a specific recognition site which, in effect, lessens its practical use for routine detection.

In this paper, a novel ultrasensitive ECL biosensor for breast-cancer marker microRNA detection based on functionalization of a quantum dot and Au nanoparticle combination and the strand-displacement property of polymerase-assisted cycles was discussed as an effective alternative to the current biosensor standards. This method is illustrated in Scheme 1. To the best of our knowledge, this study is the first to achieve microRNA biomarker detection through the amplification of target cyclic regeneration coupled with the electroluminescence of multiple quantum dot Au nanoparticles (QD-AuNPs).

Experimental

Instruments and reagents

Electrochemiluminescence detection was performed using an MPI-E Electrochemiluminescence Analysis System (Xian Ruimai Analysis Instrument Co., Ltd. http:// www. remax.testmart.cn/). CV was recorded using a CHI660D Electrochemical Workstation (Shanghai Chenhua Instrument Co., Ltd. http://www.chinstr.com/). Electrochemical Impedance spectroscopy (EIS) was performed on an Autolab Electrochemical Workstation (PGSTAT128N, Metrohm Co., Ltd. http://www.metrohm.com/). All the electrochemical measurements were carried out with the conventional three-electrode system composed of platinum wire as auxiliary, Ag/AgCl electrode as reference, and magnetically glassy carbon electrode (MGCE) as working electrode. Transmission electron microscope (TEM) images were obtained from a field transmission electron microscope (JEM-2100F, Electronics Co., Japan. https://www.jeol.co.jp/). Particle sizes were analyzed using a Zetasizer Nano-ZS-90 (Malvern Instruments Ltd., Worcestershire, UK. http://www.malvern.com.cn/). Cadmium chloride ($CdCl_2{\cdot}2.5H_2O_2$), Tellurium powder(Te), Sodium borohydride ($NaBH_4$), thioglycolic acid (TGA), and TE buffer (Tris-HCl 1 M, EDTA 1 mM) were purchased from Sinopharm Group Chemical Reagent Co., Ltd. (http://www.reagent.com.cn/). Ferrous sulfate ($FeSO_4{\cdot}7H_2O$), ferric chloride($FeCl_3{\cdot}6H_2O$), Tris-(2-carboxyethyl)-phosphine hydrochloride Potassium(TCEP), persulfate($K_2S_2O_8$), Mercaptoethanol(MCH), N-[3-(dimethylamino)propyl]-N′-ethylcarbodiimide (EDC), and N-Hydroxy succinimide(NHS) were purchased from Aladdin Co. Ltd.(http://www.alaidin-e.com/). Klenow Fragment polymerase(0.2 U μL^{-1}), 10 × enzyme reaction buffer (Tris-HCl 500 mM, 50 mM $MgCl_2$, 10 mM DTT), and deoxynucleotide triphosphates (dNTPs) mix were synthesized and purified by Sangon Biotech (Shanghai) Co., Ltd.(http://www.sangon.com/). Their sequences were listed as follows:

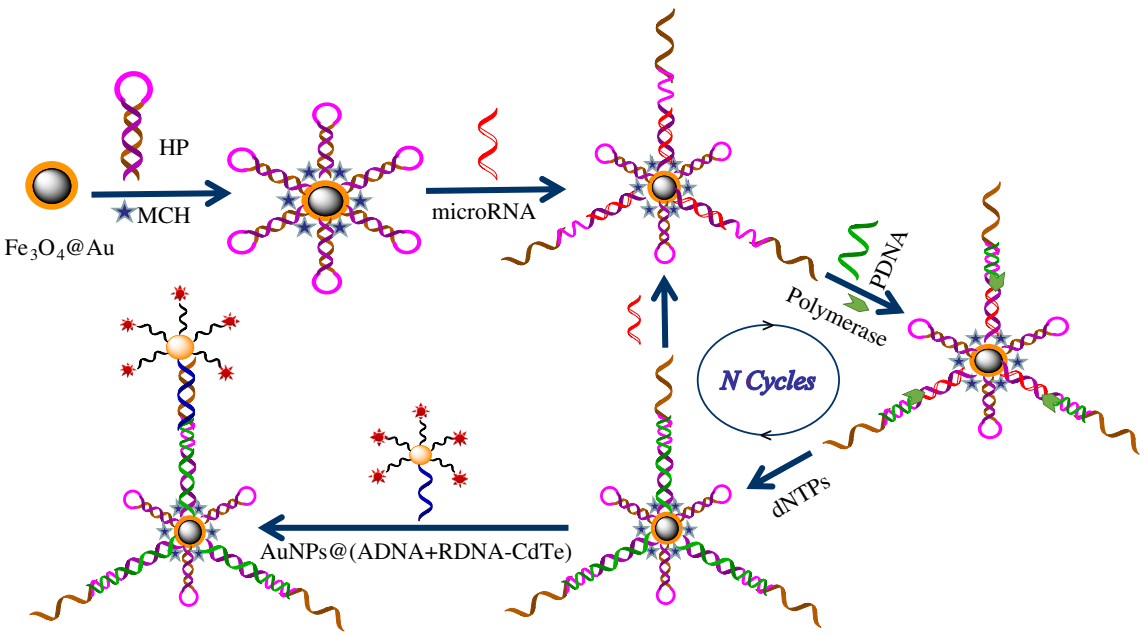

Scheme 1 Detection mechanism of the assay. HP: Hairpin probe; PDNA: Primer DNA; ADNA: Auxiliary DNA; RDNA: Reporter DNA; dNTPs: Deoxynucleotide triphosphates; MCH: Mercaptoethanol

Hairpin probe (HP): 5'-HS-C_6-CCCAGCCTTCCAGC TCCTTGGGAGCTGGAA GCTGAGCCCC-3'
Target (microRNA): 5'-CAAGGAGCUGGAAG GCUGGG-3'
Primer DNA (PDNA): 5'-AGCTCC-3'
Auxiliary DNA (ADNA): 5'-GGGGCTCAGCCTTC C-SH-3'
Reporter DNA (RDNA): 5'-NH_2-C_6-TTGTCGTG -SH-3'
Noncomplementary (microRNA 1): 5'-GGACCGCG ACCGUCCGACCC-3'
One-base mismatch (microRNA 2): 5'-CAAGGAGC AGGAAGGCUGGG-3'
Three-base mismatch (microRNA 3): 5'-CAAGGAGC AGGAACGCUGGC-3'

Preparation of magnetic Fe_3O_4@Au nanoparticles

The preparation of magnetic Fe_3O_4@Au nanoparticles was based on a previously used method [22, 23] with slight modifications. Approximately 1.14 g of $FeCl_3 \cdot 6H_2O$ and 0.67 g of $FeSO_4 \cdot 7H_2O$ were weighed and dissolved in 250 mL of double distilled water. The mixture was then poured into a three-neck flask protected by the input of nitrogen. Under rapid stirring and consistent supply of N_2 for 1.5 h at 50 °C, 2 M NaOH solution was also added to ensure a stable pH of 10. The solution was then prepared for magnetic particle development by heating to 80 °C for 30 min while the pH was maintained. The solution was then neutralized through several washes with double distilled water and absolute ethyl alcohol. Once neutralized, the solution was prepared to a concentration of 5 mg L^{-1} and stored at 4 °C for later use.

Approximately 0.229 g of sodium citrate was dissolved in 100 mL of double distilled water and then poured into another 250 mL three-neck flask for heating and stirring. Approximately 1 mL of the prepared magnetic Fe_3O_4 nanoparticles was quickly added to the sodium citrate solution when the solution was heated to 90 °C. Subsequently, 2 mL of 10 mM chloroauric acid solution was added while the solution was continuously heated and stirred for 15 min. After the heat source was removed, stirring was continued for 15 min. The resulting wine-red solution was allowed to cool to room temperature, and then magnetic separation was performed. The solution was washed with double distilled water until the pH became neutral. The Fe_3O_4@Au solution was then diluted to 20 mL after washing with double distilled water and stored at 4 °C prior to use.

Preparation of water-soluble CdTe quantum dots(TGA-CdTe)

The synthetic approach of using TGA-CdTe quantum dots was based on a previously employed method [24] with slight modifications. Approximately 250 mL of $CdCl_2$ in 0.0025 M of aqueous solution was poured into a new 250 mL three-neck flask and magnetically stirred. N_2 was passed through the solution to remove the O_2 for 15 min. Approximately 100 μL of TGA was also incorporated into the solution to roughly adjust the systematic pH level to 10. N_2 was continually passed through the solution for sealing.

Approximately 3 mL of double-distilled water was poured into a 50 mL three-neck flask and exposed to N_2 to remove O_2 in the solution. Approximately 0.144 g of Te powder and 0.36 g of $NaBH_4$ were then bathed in 65 °C water while the black Te powder was magnetically stirred until completely dissolution. As a result, a purple transparent NaHTe solution was obtained. The purple solution was mixed into the above $CdCl_2$ aqueous solution by stirring and refluxing, finally obtaining the desired wine-red CdTe quantum dot solution.

Preparation of gold nanoparticles (AuNPs)

The AuNPs were synthesized following a previously employed methodology [25]. Approximately 100 mL of 1 M $HAuCl_4$ was added into a 250 mL three-necked flask. After vigorously stirred, 3 mL of 1 M sodium citrate was added. The mixture was then boiled for 30 min to obtain the wine-red colored AuNPs and stored at 4 °C for later use.

Preparation of DNA-functionalized AuNPs (AuNPs@ADNA)

Auxiliary DNA (ADNA) was labeled and performed in accordance with a previous study [26]. A mixture of 10 μM DNA (ADNA) was activated with the addition of 10 μL of 10 mM TCEP. After incubation for 1 h, 1 mL of freshly-prepared AuNPs was added and gently shaken overnight. After 16 h, the AuNPs@ADNA conjugates was aged in salts for 24 h. Excess reagents were then removed by centrifugation at 16,000 rpm for 30 min. The red precipitate was washed and centrifuged three times. The resulting NPs were dispersed into a buffer solution and stored at 4 °C.

Modification of reporter DNA (RDNA) with AuNPs@ADNA and TGA–CdTe

Approximately 100 mL of 50 mg mL^{-1} NHS solution and 20 mg mL^{-1} EDC of TGA–CdTe were added to Reporter DNA (RDNA)-functionalized AuNPs@ADNA (AuNPs@ADNA+RDNA-CdTe) and incubated at room temperature for 24 h with gentle shaking. The RDNA was then tagged with AuNPs@ANA and TGA–CdTe were collected by centrifugation at 10,000 rpm for

30 min. Finally, the precipitate was washed, resuspended in water, and stored at 4 °C for later use.

Assay procedure

Magnetically glassy carbon electrode (MGCE) was fully polished with 0.05 μM alumina powder, washed separately with double-distilled water and ethanol, and dried with N_2 blow. The MGCE was then scanned by cyclic voltammetry from −0.2 to +0.6 V in 0.05 M $[Fe(CN)_6]^{3-/4-}$ until the voltammograms became stable. Finally, the electrode was cleaned with double-distilled water and ethanol for later use.

Approximately 10 μL of prepared Fe_3O_4@Au was then exposed to the electrode. Prior to attachment onto the electrode surface, thiolated HP was incubated with 10 mM TCEP for 1 h to reduce disulfide bonding, diluted to 1.0 μM with TE buffer, and incubated overnight at 37 °C. The surface of the electrode was then rinsed with double-distilled water. To decrease background signals, we immersed the electrode in 1 mM MCH at 37 °C for 1 h to block nonspecific binding

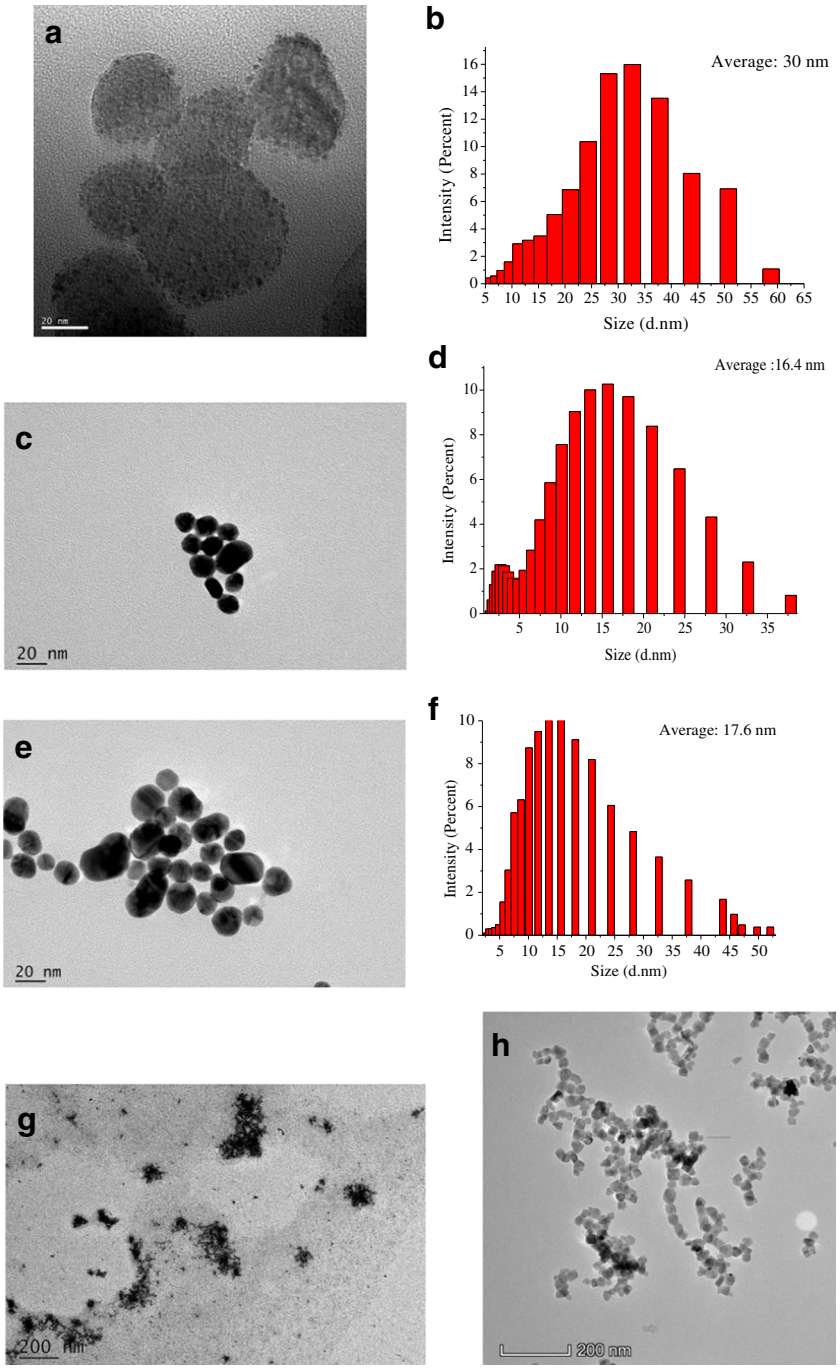

Fig. 1 TEM images (**a**, **c**, **e**, **g**, **h**) and particle size distributions (**b**, **d**, **f**). (**a**) and (**b**): Fe_3O_4@Au; (**c**) and (**d**): TGA-CdTe QDs; (**e**) and (**f**): AuNPs; (**g**): QDs-DNA-AuNPs; (**h**): QDs-AuNPs/polymerase/microRNA/HP/MCH/Fe_3O_4@Au

sites with the potential to produce nonspecific HP adsorption. The HP probe-modified electrode was obtained and was exposed to a series of 10 μL of target microRNA mixtures of different concentrations at 37 °C for 1 h. Subsequently, 50 μL of polymerase solution containing 10 μM primer DNA, 4 U of Klenow fragment (3′ → 5′exo⁻), 0.5 nM of dNTPs, and 10× enzyme reaction buffer was exposed to the modified electrode. After 37 °C was reached for 2 h, the electrode was rinsed thoroughly with washing double-distilled water. The modification of signal DNA probe with AuNPs and TGA-CdTe was activated in 50 μL of solution at 37 °C for 60 min, and the electrode was subsequently washed with double-distilled water.

Electrochemical measurements

The ECL intensity on different concentrations of target microRNA was recorded by using a MPI-E electrochemiluminescence analysis system within a potential range of −1.8–0.0 V (vs. Ag/AgCl), the scanning speed was set to 100 mV s^{-1}, the photomultiplier tube was set to a max voltage of 900 V, and the supporting electrolyte solution consisted of 0.1 M phosphate buffer saline (pH 7.4) containing 0.1 M $K_2S_2O_8$ and 0.1 M KCl. Cyclic voltammetry (CV) measurement was performed in the solution of 0.1 M KCl and 0.05 M $[Fe(CN)_6]^{3-/4-}$, potentials were scanned from −0.2 to +0.6 V (vs. Ag/AgCl) at a scan rate of 0.1 V s^{-1}. Electrochemical impedance spectroscopy (EIS) was performed in the same solution as mentioned above with 0.19 V impedance potential, 5 mV amplitude, and 0.1–100,000 Hz frequency range.

Results and discussion

TEM and particle size characterization

The morphology of the synthesized Fe_3O_4@Au, TGA-CdTe QDs, AuNPs, QDs-DNA-AuNPs, and QDs-AuNPs/polymerase/microRNA/HP/MCH/Fe_3O_4@Au were evaluated by TEM, and the particle sizes of Fe_3O_4@Au, TGA-CdTe QDs, and AuNPs were measured by a size analyzer. Figure 1a shows a TEM image of Fe_3O_4@Au magnetic nanoparticles, which illustrates the uniform dispersion of the nanoparticles in an average diameter of approximately 30 nm and with AuNPs coated on the outer layer of Fe_3O_4. Figure 1c, e show the image of CdTe QDs and AuNPs respectively, which distinctly indicate uniform size distributions with quasi-spherical structure. The average sizes of Fe_3O_4@Au, TGA-CdTe QDs, and AuNPs particles were around 30 nm, 16.4 nm, and 17.6 nm separately as illustrated in Fig. 1b, d, f. The particles size analyses are consistent with the results from TEM observation, which demonstrates that nanoparticles were successfully synthesized. With the presence of ADNA and RDNA, large

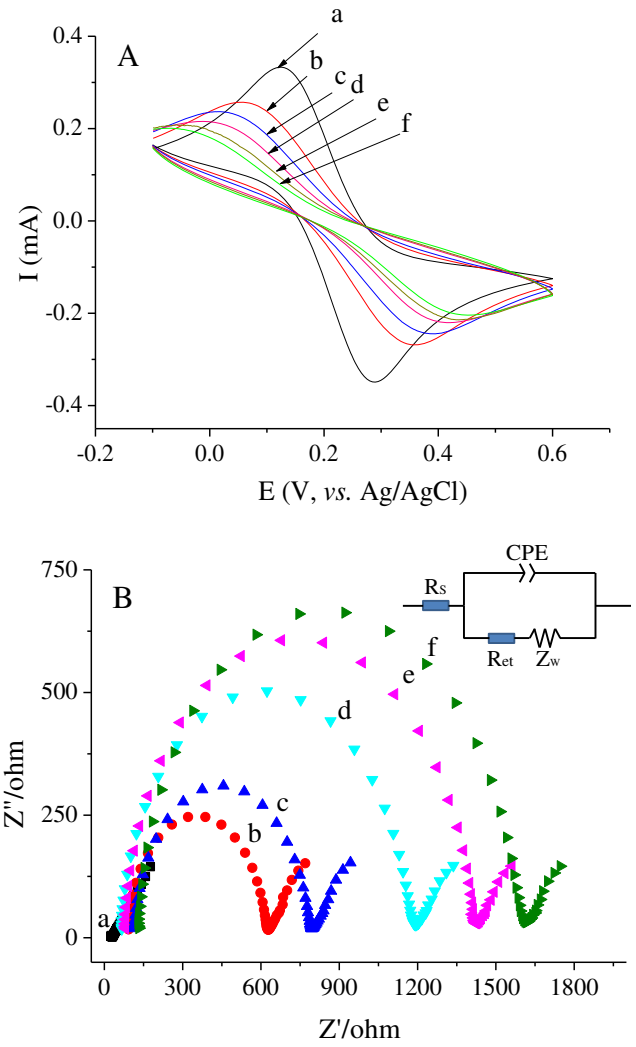

Fig. 2 (**a**) Cyclic voltammograms and (**b**) AC impedances curves of modification processes recorded at (a) MGCE; (b) Fe_3O_4@Au/MGCE; (c) HP/MCH/Fe_3O_4@Au/MGCE; (d) microRNA/HP/MCH/Fe_3O_4@Au/MGCE; (e) polymerase/microRNA/HP/MCH/Fe_3O_4@Au/MGCE; (f) QDs-AuNP/polymerase/microRNA/HP/MCH/Fe_3O_4@Au/MGCE in electrolyte containing 0.1 M KCl and 5 mM $[Fe(CN)_6]^{3-/4-}$ with scan rate of 100 mV s^{-1}. Inset figure is the equivalent circuit applied to fit the impedance data

clusters of QDs-DNA-AuNPs were formed since AuNPs and QDs aggregated (Fig.1g). When DNA probe was added into the solution containing dNTPs/PDNA/polymerase/microRNA/HP/MCH/Fe_3O_4@Au, as can be seen from Fig.1h, the nanoparticle-DNA-concatemer-like structure formed, which further demonstrates that the amplified ECL signal of this biosensor can be measured.

CV and AC characterization of the electrode modification

CV is an effective method for monitoring the changes in the surface features of the modified electrodes. Figure 2a shows

the assembly processes observed by cyclic voltammetry with a 5 mM ferricyanide ion probe. Curve (a) presents the cyclic voltammogram of $[Fe(CN)_6]^{3-/4-}$ on a bare electrode. When Fe_3O_4@Au was modified on the electrode, peak current significantly decreased, as shown in curve (b), due to the hindering of charge transfers. When the electrode was blocked with HP, the peak current further decreased, as shown in curve (c), due to HP being partially adsorbed onto the electrode surface. Curve (d) illustrates another decrease in the peak current of the CV due to microRNA modification on the electrode. This effect was the result of microRNA increasing the negative charge density of the electrode surface and hindering the transfer of charge. After the formation of long double helices by strand replacement polymerization via substituting microRNA on the electrode, the large negatively charged DNA block appeared, further inhibiting the mass transfer of charge. The resulting increase in the smaller peak current is illustrated in Curve (e). Finally, the integration of AuNPs enhanced CdTe, which corresponded with the results of further decreased peak current in the CV, as illustrated in Curve (f). The marked change suggests the successful immobilization and adsorption on the surface of the electrode.

EIS is a frequently-used tool to investigate the interface properties of the modified electrodes in the assembly process. Figure 2b shows the EIS Nyquist plot observed through the stepwise modification. The inset in Fig. 2b is the equivalent circuit applied to fit the impedance data. R_s is solution resistance, CPE is constant phase angle element, Z_w is Warburg diffusion resistance, and the semicircle diameter of impedance represents the electron transfer resistance (R_{et}), which directly controls the electron transfer kinetics of the redox probe at the electrode interface. The bare electrode is represented by a small semicircle diameter of EIS Nyquist plot (Curve a) which indicates a low R_{et} value of the redox coupling. Significant increases in R_{et} values were also observed due to the immobilization of Fe_3O_4@Au (Curve b). The modification of HP on the electrode surface further inhibited the transfer of charge (Curve c) due to the negative charge on the phosphate backbone of HP interfering with the movements of $[Fe(CN)_6]^{3-/4-}$. When the electrode was treated with microRNA, charge transfer resistance on the electrode surface increased (Curve d). Then an increase of R_{et} was observed (curve e) after the strand replacement polymerization due to long amplified DNA products being captured on the electrode surface. Finally, the connection between AuNPs and DNA enabled the enhancement of CdTe, which corresponded with the blocking of the charge transfer of the $[Fe(CN)_6]^{3-/4-}$ redox system and led to a significant increase of R_{et}. The result of EIS confirms the successful immobilization of magnetic particles onto the surface of the electrode.

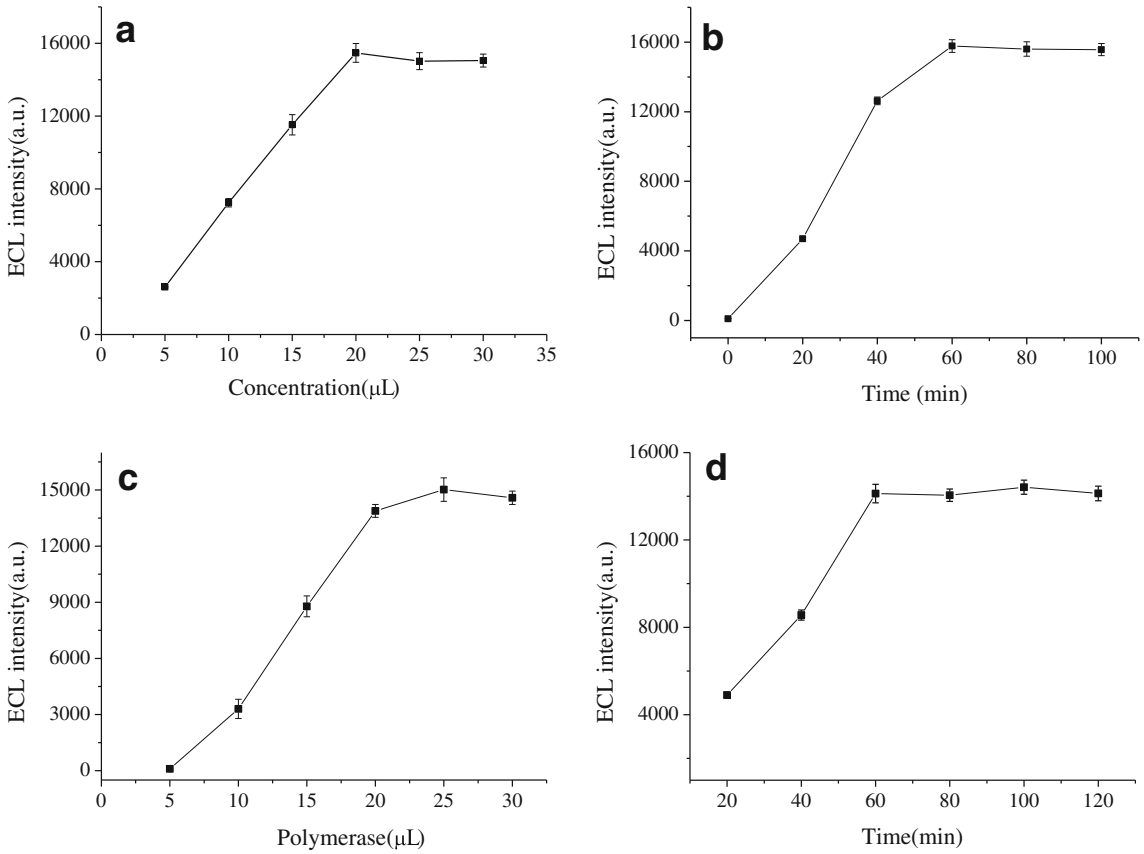

Fig. 3 Effects of (**a**) the volume of Fe_3O_4, (**b**) hybridization time of target microRNA, (**c**) volume of polymerase, and (**d**) hybridization time of QDs-AuNP and auxiliary probe on the ECL intensity

Optimization of analytical parameters

Fe_3O_4@Au concentration heavily affected the effectiveness of the signal. As shown in Fig. 3a, ECL signal increased and gradually stabilized with the increase in Fe_3O_4@Au concentration, and optimization occurred specifically at 20 μL. Figure 3b also demonstrates that the ECL signal can increase, gradually stabilize, and then reaches at 60 min, indicating the completion of the hybridization between the complementary microRNA and HP. Thus, 60 min was the preferred hybridization time. The greater number of repeated sequences produced by circular strand replacement polymerization, the greater was the amount of the ECL signal on the electrode. With an increase in the amount of polymerase, the ECL signal also gradually increased. However, the signal reached equilibrium after the amount of polymerase reached 20 μL. Therefore, Fig. 3c demonstrates that the dosage of enzyme used for reactions was 20 μL. The hybridization reaction time between QDs-AuNP and the auxiliary probe is another key variable of the experiment. As shown in Fig. 3d, the experiment duration with hybrid time was 60 min.

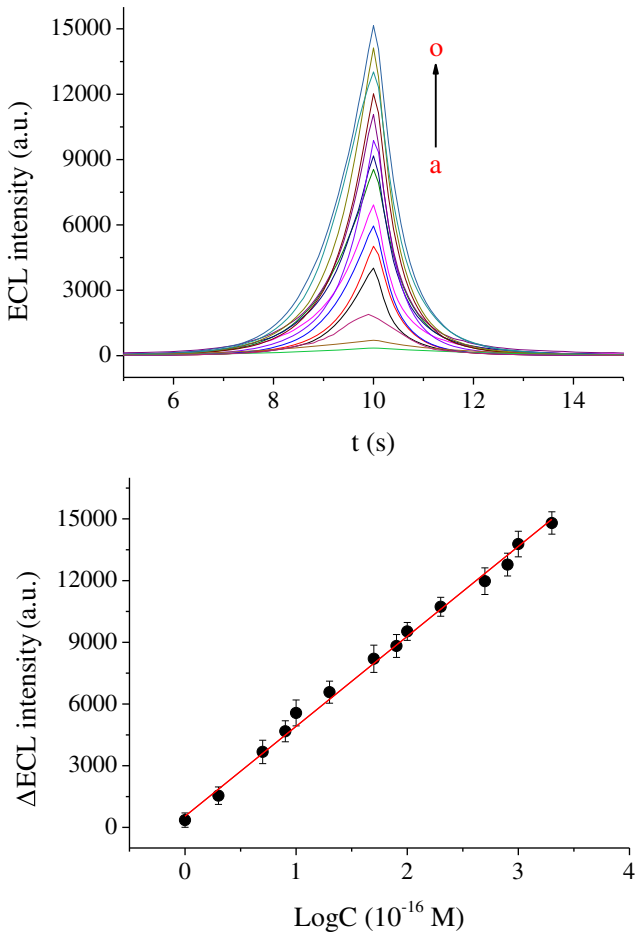

Fig. 4 ECL intensity of biosensor at different microRNA concentrations versus time and the calibration plot, from a to o: 0, 1, 2, 5, 8, 10, 20, 50, 80, 100, 200, 500, 800, 1000, and 2000 × 10^{-16} M

Table 1 Comparison of performance of different biosensors

Detection methods	Linear range(M)	Detection limit (M)	Reference
Fluorescence	5.0×10^{-9}–2.0×10^{-7}	2.4×10^{-9}	[27]
Rolling circle amplification	1.0×10^{-13}–1.0×10^{-8}	2.23×10^{-14}	[28]
Enzyme-amplified	5.0×10^{-11}–5.0×10^{-9}	8.4×10^{-14}	[29]
Exonuclease III-assisted	2.0×10^{-14}–2.0×10^{-9}	1.28×10^{-14}	[30]
QDs–AuNP	1.0×10^{-16}–2.0×10^{-13}	3.3×10^{-17}	This work

– not given

Calibration plot

Under optimal conditions, ECL was used to detect microRNA after the modified electrode was placed in a microRNA solution of different concentrations. Figure 4 displays the ECL intensity of microRNA biosensor with different types of target microRNA. As shown in Fig. 4, the increase in microRNA concentration was correlated with ECL signal improvement, as demonstrated by the linear relationship between the ECL signal (a.u.) and microRNA concentration (lg*C*) within a range of 0.1 fM to 0.2 pM. The linear regression equation is $\Delta I = 541.8 + 4374.2\ \lg C(10^{-16}\ M)$ with an R^2 value of 0.996, indicating a good linear relationship between the test ranges. A detection limit of 33 aM was achieved, and this limit was also lower than the limits reported in other studies (Table 1).

Selectivity, stability, and reproducibility

The selectivity of the present ECL biosensor was challenged with four similar strands that included a target microRNA (a), a single-base mismatch strand of microRNA (b), a non-complementary strand of microRNA (c), a triple-base mismatch of microRNA (d), and an additional blank sample (e).

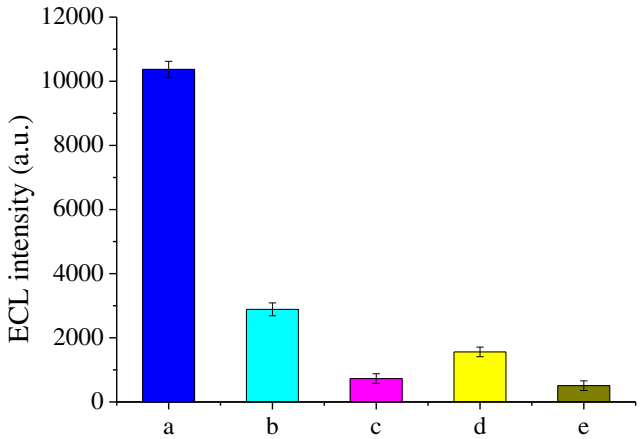

Fig. 5 Selectivity of the microRNA biosensor. (**a**) target microRNA; (**b**) single-base mismatch strand of microRNA; (**c**) non-complementary strand of microRNA; (**d**) triple-base mismatch of microRNA; (**e**) blank

Table 2 Determination of microRNA in the serum samples

Samples	Found (fM)	Added (fM)	Total found (fM)	RSD (%, $n = 5$)	Recovery (%)
1	Not found	0.500	0.478	4.30	95.6
2	Not found	2.00	2.01	3.20	100.5
3	Not found	8.00	7.55	2.60	94.4

As Fig. 5 illustrates, the ECL response of target microRNA was obviously larger than those of other three microRNA strands when tested in the same concentration (10^{-13} M) of microRNA strands. This demonstrates that single-base mismatch strand (b), non-complementary strand (c), triple-base mismatch strand (d), and blank (e) all show slight interference when detecting the target microRNA. These results also suggest that the biosensor can effectively detect all targets with high selectivity.

The reproducibility of this method was also evaluated. The results show that the ECL intensity did not significantly change within 10 days (ECL signal change within ±5%), and was reduced by 6.70% within 20 days. The results also show the reliable stability of the sensor. Five sensors were prepared to test the microRNA under the same conditions, and the determination results of relative standard deviation were 2.37% for all of the samples. This consistency demonstrated the good stability and reliability of the proposed strategy.

Determination of microRNA in serum samples

To test the generality of the proposed assay in a clinical sample, recovery testing was carried out by spiking human serum from the Guilin University of Technology Hospital with microRNA solution. The results are shown in Table 2. The recovery rate of the proposed electrochemical sensor was within the range of 94.4% to 100.5%, with an RSD of less than 5%. The results indicate that the established assay is desirable and qualified for practical sample testing.

Conclusions

The ultrasensitive electroluminescence biosensor for breast-cancer cell microRNA detection described here is based on cyclic regeneration and multilabeled AuNPs, which was designed to work in conjunction with a hairpin-shaped capture probe to identify the polymerase circle amplification coupling with the AuNPs@(ADNA+RDNA-CdTe). This procedure can be extended to medical settings to improve diagnosis and approach to deciding therapeutic courses. Practical analysis is also recommended to further improve the efficiency and accuracy of this method.

Acknowledgements The authors gratefully acknowledge the financial support from National Natural Science Foundation of China (No. 21765006), the Natural Science Foundation of Guangxi Province of China (2015GXNSFFA139005; 2018GXNSFAA050023), Guangxi Colleges and Universities Key Laboratory of Food Safety and Detection, High Level Innovation Teams of Guangxi Colleges & Universities and Outstanding Scholars Program (Guijiaoren[2014]49) for this research project.

Compliance with ethical standards The author(s) declare that they have no competing interests.

Ethical standards and informed consent The study and experimental sections were approved by the Hospital of Guilin University of Technology. Human serum samples used in this study do not have any identifying information about all the participants that provided written informed consent.

References

1. Teengam P, Siangproh W, Tuantranont A, Vilaivan T, Chailapakul O, Henry CS (2018) Electrochemical impedance-based DNA sensor using pyrrolidinyl peptide nucleic acids for tuberculosis detection. Anal Chim Acta 1044:102–109
2. Schulz D, Zanotelli VRT, Fischer JR, Schapiro D, Engler S, Lun XK, Jackson HW, Bodenmiller (2018) Simultaneous multiplexed imaging of mRNA and proteins with subcellular resolution in breast Cancer tissue samples by mass cytometry. Cell Syst 6:25–36
3. Hirschberger K, Jarzebinska A, Kessel E, Kretzschmann V, Aneja MK, Dohmen C, Herrmann-Janson A, Wagner E, Plank C, Rudolph C (2018) Exploring cytotoxic mRNAs as a novel class of anti-cancer biotherapeutics. Mol Ther-Meth Clin D 8:141–151
4. Zhao B, Zhao Y, Sun Y, Niu HT, Sheng L, Huang DF, Li L (2018) Alterations in mRNA profiles of trastuzumab-resistant Her-2-positive breast cancer. Mol Med Rep 18:139–146
5. Antonio MD, Tamayo P, Mesirov JP, Frazer KA (2016) Kataegis expression signature in breast cancer is associated with late onset, better prognosis, and higher HER2 levels. Cell Rep 16:672–683
6. Imani S, Zhang X, Hosseinifard H, Fu SY, Fu JJ (2017) The diagnostic role of microRNA-34a in breast cancer: a systematic review and meta-analysis. Oncotarget 8:23177–23187
7. Zhang HY, Liang F, Zhang JW, Wang F, Wang L, Kang XG (2017) Effects of long noncoding RNA-ROR on tamoxifen resistance of breast cancer cells by regulating microRNA-205. Cancer Chemother Pharmacol 79:327–337
8. Vilela P, El–Sagheer A, Millar TM, Brown T, Muskens OL, Kanaras AG (2017) Graphene oxide-Upconversion nanoparticle based optical sensors for targeted detection of mRNA biomarkers present in Alzheimer's disease and prostate Cancer. ACS Sens 2:52–56
9. Trayhurn P, Duncan JS, Nestor A, Thomas MEA, Eastmond NC, Vernon RD (2010) Rapid chemiluminescent detection of mRNAs on northern blots with digoxigenin end-labelled oligonucleotides. Electrophoresis 16:341–344
10. Lee JM, Cho H, Jung Y (2016) Fabrication of a structure-specific RNA binder for Array detection of label-free MicroRNA. Angew Chem Int Edit 49:8662–8665
11. Zhang M, Zhou FY, Zhou DQ, Chen DL, Hai H, Li JP (2019) An aptamer biosensor for leukemia marker mRNA detection based on polymerase-assisted signal amplification and aggregation of illuminator. Anal Bioanal Chem 411:139–146

12. Cassol D, Cruz FP, Espindola K, Espindola K, Mangeon A, Muller C, Loureiro ME, Correa RL, Sachetto-Martins G (2016) Identification of reference genes for quantitative RT-PCR analysis of microRNAs and mRNAs in castor bean (Ricinus communis L.) under drought stress. Plant Physiol Biochem 106:101–107
13. He L, Lu DQ, Liang H, Xie ST, Luo C, Hu MM, Xu LJ, Zhang XB, Tan WH (2017) Fluorescence resonance energy transfer-based DNA tetrahedron nanotweezer for highly reliable detection of tumor-related mRNA in living cells. ACS Nano 11:4060–4066
14. Luan M, Li N, Pan W, Yang L, Yu Z, Tang B (2016) Simultaneous detection of multiple targets involved in the PI3K/AKT pathway for investigating cellular migration and invasion with a multicolor fluorescent nanoprobe. Chem Commun 53:356–359
15. Liu RJ, Zhao JJ, Huang ZR, Zhang LL, Shi BF, Zou MB, Zhao SL (2017) Nitrogen and phosphorus co-doped graphene quantum dots as a nano-sensor for highly sensitive and selective imaging detection of nitrite in live cell. Sensors Actuators B Chem 240:604–612
16. Ban F, Shi H, Feng C, Mao X, Yin Y, Zhu X (2016) A one-pot strategy for the detection of proteins based on sterically and allosterically tunable hybridization chain reaction. Biosens Bioelectron 86:219–224
17. Yu X, Zhang ZL, Zheng SY (2015) Highly sensitive DNA detection using cascade amplification strategy based on hybridization chain reaction and enzyme-induced metallization. Biosens Bioelectron 66:520–526
18. Zhang KY, Lv SZ, Lin ZZ, Li MJ, Tang DP (2018) Bio-barcode-based photoelectrochemical immunoassay for sensitive detection of prostate-specific antigen using rolling circle amplification and enzymatic biocatalytic precipitation. Biosens Bioelectron 101:159–166
19. Shen QM, Fan MX, Yang Y, Zhang H (2016) Electrochemical DNA sensor–based strategy for sensitive detection of DNA demethylation and DNA demethylase activity. Anal Chim Acta 934:66–71
20. Huang KJ, Shuai HL, Zhang JZ (2016) Ultrasensitive sensing platform for platelet-derived growth factor BB detection based on layered molybdenum selenide–graphene composites and ExonucleaseIII assisted signal amplification. Biosens Bioelectron 77:69–75
21. Gan XR, Zhao HM, Chen S, Quan X (2015) Electrochemical DNA sensor for specific detection of picomolar hg (II) based on exonuclease III-assisted recycling signal amplification. Analyst 140:2029–2036
22. Zhou FY, Hai H, Yuan YL, Li JP (2017) Ultrasensitive Electrochemiluminescence biosensor for mRNA based on polymerase assisted signal amplification. Electroanal 29:983–989
23. Wang LP, Huang YB, Lai H (2018) Surface enhanced Raman scattering activity of dual-functional Fe_3O_4/Au composites. Appl Surf Sci 435:290–296
24. Xue M, Wang W (2016) Facile one-pot synthesis of water-soluble β-cyclodextrin coated CdTe quantum dots. Mater Lett 166:97–100
25. Murayama T, Haruta M (2016) Preparation of gold nanoparticles supported on Nb_2O_5 by deposition precipitation and deposition reduction methods and their catalytic activity for CO oxidation. Chin J Catal 37:1694–1701
26. Jackson SR, Wong AC, Travis AR, Catrina IE, Bratu DP, Wright DW, Jayagopal A (2016) Chapter four–applications of hairpin DNA-functionalized gold nanoparticles for imaging mRNA in living cells. Methods Enzymol 572:87–103
27. Zhang XF, Xu HM, Han L, Li NB, Luo HQ (2018) A Thioflavin T-induced G-Quadruplex fluorescent biosensor for target DNA detection. Anal Sci 34:149–153
28. Lee CY, Fan HT, Hsieh YZ (2018) Disposable aptasensor combining functional magnetic nanoparticles with rolling circle amplification for the detection of prostate-specific antigen. Sensors Actuators B Chem 255:341–347
29. Lei Y, Wang K, Wu SY, Huang DD, Dai M, Zheng YJ, Sun ZL, Chen YZ, Lin XH, Liu AL (2018) 2'-Fluoro ribonucleic acid modified DNA dual-probe sensing strategy for enzyme-amplified electrochemical detection of double-strand DNA of PML/RARα related fusion gene. Biosens Bioelectron 112:170–176
30. Ma RN, Wang LL, Wang HF, Jia LP, Zhang W, Shang L, Xue QW, Jia WL, Liu QY, Wang HS (2018) Highly sensitive ratiometric electrochemical DNA biosensor based on homogeneous exonuclease III-assisted target recycling amplification and one-step triggered dual-signal output. Sensors Actuators B Chem 269:173–179